

SED and Galactic kinematic diagnostics for dormant BH/NS binary candidates

QIAN-YU AN  ¹ AND WEI-MIN GU  ¹¹ Department of Astronomy, Xiamen University, Xiamen, Fujian 361005, People's Republic of China

ABSTRACT

The third data release of the *Gaia* mission (*Gaia* DR3) has enabled large-scale searches for dormant black hole and neutron star binaries with stellar companions at wide separations. A recent study has proposed thousands of dormant black hole and neutron star binary candidates using summary statistics from *Gaia* DR3 by simulating and fitting *Gaia* observables. In this Letter, we perform broadband spectral energy distribution (SED) fitting from the optical to the infrared for 1,328 candidates, incorporating GALEX ultraviolet photometry to assess the presence of hidden hot companions. We quantify ultraviolet excess by comparing observed near-ultraviolet fluxes with single-star SED predictions and further test whether excesses can be explained by non-degenerate stellar companions for sources exhibiting moderate excess. We additionally examine the Galactic kinematics of the sample to identify systems potentially affected by natal kicks during compact-object formation. By combining the ultraviolet and kinematic diagnostics, we identify 176 sources as the highest-priority candidates for follow-up observations, in which 19 are black hole candidates with previously provided masses $\geq 3 M_{\odot}$.

1. INTRODUCTION

Theoretical models suggest the Milky Way harbors billions of black holes (BHs) and neutron stars (NSs) (e.g. F. X. Timmes et al. 1996; N. Sartore et al. 2010), driving decades-long searches for these objects. Historically, accreting BH X-ray binaries have been primarily discovered since the 1960s through their characteristic X-ray bursts, leading to the identification of ~ 30 accreting BH X-ray binaries (e.g. J. M. Corral-Santana et al. 2016). NS searches have employed both X-ray bursts and radio pulse detections, yielding hundreds of detections via X-ray bursts (e.g. F. Fortin et al. 2024) and thousands via radio pulses (R. N. Manchester et al. 2005).

However, these classical methods sampled only a small fraction of the total BH and NS population. X-ray burst detections prefer accreting BHs/NSs, while radio pulse detections can only detect rapidly rotating NSs which emit electromagnetic pulse signals beaming towards us. Recent technological advances and data accumulation have spurred the development of novel search techniques. Microlensing remains the only currently feasible method for detecting isolated stellar-mass BHs, yielding several candidates (e.g. L. Wyrzykowski et al. 2016) and one confirmed detection (K. C. Sahu et al. 2025). With the detection of GW150914 (B. P. Abbott et al. 2016), gravitational wave observations are dedicatedly revealing merging BH-BH and BH-NS binaries, and more than 300 events have been detected (The LIGO Scientific Collaboration et al. 2025). Furthermore, large-scale spectroscopy surveys have amassed vast stellar spectral datasets, enabling the identification of non-accreting BHs and NSs in medium-to-short orbital period binaries through radial velocity (RV) monitoring (e.g. L. Mahy et al. 2022; T. Yi et al. 2022).

While discoveries from these novel methods have expanded the known populations of BHs and NSs, they have yet to significantly increase their total known numbers. Importantly, the third data release of the *Gaia* mission (*Gaia* DR3; Gaia Collaboration et al. 2023) offers a promising new avenue to overcome this limitation. Its initial data release included orbital solutions for 1.7×10^5 binaries with full astrometric parameters. Utilizing these full astrometric solutions along with spectroscopic observations, BHs and NSs in (ultra-)wide binaries are being revealed (e.g. K. El-Badry et al. 2023a,b; S. Wang et al. 2024). However, only a small fraction of wide binaries have full astrometric solutions due to the stringent quality cuts, inevitably missing detections for many BHs and NSs in wide binaries. To

address this, J. Müller-Horn et al. (2025) extended their search beyond binaries with full orbital solutions to the entire *Gaia* DR3 dataset. They employed a forward-modeling framework, simulating *Gaia* observables for 21,028 red-giant branch (RGB) stars to target massive dark companions, yielding 556 RGB + BH candidates.

Assessing the risk of hidden hot companions is necessary for these candidates, given previous false alarms like J0521 and V723 Mon. Both systems were initially reported as RGB + BH binaries (T. A. Thompson et al. 2019; T. Jayasinghe et al. 2021), but were later revealed via ultraviolet (UV) features to host hot companions (L. Bianchi et al. 2024; C. S. Kochanek et al. 2025). While UV excess provides a powerful diagnostic for identifying hot luminous stellar contaminants, kinematic signatures offer an independent probe of compact-object formation. Supernova explosions associated with the birth of BHs or NSs can impart substantial natal kicks to binary systems through asymmetric mass loss and explosion kinematics, leading to significantly heated binary orbits and high peculiar velocities (V_{pec}) (e.g. A. Blaauw 1961; A. G. Lyne & D. R. Lorimer 1994; G. Hobbs et al. 2005; H.-T. Janka 2013). Kinematic information therefore provides a complementary avenue to distinguish genuine compact-object binaries from ordinary stellar systems.

In this work, we perform spectral energy distribution (SED) analysis for 1,328 sources from J. Müller-Horn et al. (2025), along with Galactic kinematic analysis, as a reference for evaluating their reliability and priority selection of follow-up observation sources. The structure of this paper is organized as follows. In Section 2, we introduce the source selection for analysis in this work and corresponding data collection. In Section 3, we introduce our SED fitting method and use UV diagnostics to select sources. In Section 4, we analyze the Galactic kinematics of our sample. We summarize our results and make a discussion in Section 5.

2. SOURCE SELECTION AND DATA COLLECTION

Our initial sample comprises 3,773 sources with `fit_companion_mass` $\geq 1.4 M_{\odot}$ and `flag_quality == True`. Due to the necessity of UV diagnostics to evaluate the risk of hidden hot companions, we refine sources by requiring available UV photometry. The Galaxy Evolution Explorer (GALEX) (D. C. Martin et al. 2005; P. Morrissey et al. 2005) is uniquely useful for this purpose, being the only modern mission that performed a large-area, UV photometric imaging survey of the sky with high spatial resolution. Equipped with a 50-cm Ritchey–Chrétien telescope, GALEX can simultaneously observe in two broadband channels—the far-ultraviolet (FUV; 1,350–1,750 Å) and near-ultraviolet (NUV; 1,750–2,750 Å). GALEX General Releases 6 and 7 (GR6/GR7) constituted the most complete and final public data products from the mission, containing 82,992,086 sources, so we cross-match our sample with GALEX GR6/GR7 to acquire UV photometry. This reduces the sample to 903 sources. Additionally, we retrieve the Merged Catalog of Sources (`AIS_*_mcat.fits`) by python codes `from astroquery.mast import Catalogs` and `Catalogs.query_region()` (A. Ginsburg et al. 2019), which provides UV photometry for another 645 sources.

To construct the broadband SED, we supplement photometry from existing *Gaia* G, BP and RP bands by retrieving the archive of The AAVSO Photometric All-Sky Survey (APASS) (g , r , i , B and V bands; A. A. Henden et al. 2015), Transiting Exoplanet Survey Satellite (*TESS*) (T band; G. R. Ricker et al. 2015), Two Micron All-Sky Survey (2MASS) (J , H and K bands; M. F. Skrutskie et al. 2006) and Wide-field Infrared Survey Explorer ($W1$ and $W2$ bands; E. L. Wright et al. 2010), to collect optical and infrared photometry. Sources retrieved in APASS may only have photometry for partial bands, and we only reserve sources with at least three bands of photometry to ensure enough photometric data points. Finally, we filter sources with `parallax_over_err < 5`, leaving 1,349 sources.

Given the inherent degeneracies in SED fitting, incorporating priors on stellar parameters is essential. We adopt stellar parameters published by D. Huson et al. (2025a), who have developed a new pipeline, *Gaia* Net, for reprocessing *Gaia* XP spectra, to predict stellar parameters for 220 million stars released in *Gaia* DR3 and published their results on Vizier² (F. Ochsenbein et al. 2000; D. Huson et al. 2025b), due to the complete sample coverage and accessibility. 21 sources without uncertainties for all three stellar parameters have been ruled out in this process, assigning 1,328 sources for the following studies.

3. SED FITTING

We set an additional systematic photometric uncertainty of 0.03 mag for each band, then we fit the SEDs with a single-star model. Photometry data used for SED fitting do not contain UV photometry data from GALEX. The parameters for SED fitting include effective temperature T_{eff} , surface gravity $\log g$, metallicity [Fe/H], stellar radius

² <https://vizier.cds.unistra.fr/viz-bin/VizieR?-source=J/ApJ/984/58>

R , distance D , and V -band extinction A_V . We perform the SED fitting using an affine-invariant Markov Chain Monte Carlo sampler implemented in `emcee` (D. Foreman-Mackey et al. 2013) to explore the posterior distribution of the model parameters. The posterior probability of the fitting parameters P_{rob} is denoted as:

$$\ln P_{\text{rob}} = \ln \mathcal{L} + \ln \mathcal{P}, \quad (1)$$

where \mathcal{L} is the likelihood and \mathcal{P} is prior. We adopt separable priors for all model parameters. Gaussian priors are applied to T_{eff} , $\log g$, and $[\text{Fe}/\text{H}]$ based on *Gaia* Net estimates, while the prior of D is informed by the *Gaia* parallax. A_V and R are assigned non-informative flat priors over their physically allowed ranges. The likelihood \mathcal{L} is denoted as:

$$\ln \mathcal{L} = -\frac{1}{2} \sum_{\text{band}} \left(\frac{F_{\text{obs,band}} - F_{\text{mod,band}}(T_{\text{eff}}, \log g, [\text{Fe}/\text{H}], R, D, A_V)}{\sigma_{\text{obs}}} \right)^2 \quad (2)$$

where $F_{\text{obs,band}}$ is the observed flux, $F_{\text{mod,band}}$ is the model flux, and σ_{obs} is the error of the observed flux. For each set of fitting parameters, the model flux of each band is calculated by convolving the synthetic spectrum with the corresponding transmission curve provided by the virtual observatory SED analyzer³ (VOSA) (A. Bayo et al. 2008). The synthetic spectrum is generated by `pystellib`⁴ for a given set of $(T_{\text{eff}}, \log g, [\text{Fe}/\text{H}], R)$, using `BTSettl` library (F. Allard et al. 2001, 2012; F. Allard 2016), then reddened according to the Fitzpatrick extinction law (E. L. Fitzpatrick 1999). The total-to-selective extinction ratio R_V is set to be 3.1 (J. A. Cardelli et al. 1989) and the reddening coefficients at different wavelengths for a given A_V are calculated by `extinction` (K. Barbary 2016). Finally, the synthetic spectrum is diluted by $4\pi D^2$. The zero-point used for converting magnitude to flux of each band is also provided by VOSA.

For each source, we adopt the median of the posterior distribution for each parameter as the best-fitting value and generate the corresponding synthetic spectrum. We then compute the reduced χ^2 of the fit using all non-UV photometric bands. To ensure that the observed broadband photometry is adequately described by a single-star SED model, we retain only sources whose reduced χ^2 corresponds to a goodness-of-fit probability $p > 0.05$, given the appropriate degrees of freedom. As a result, 195 sources are excluded, yielding a cleaner sample containing 1,133 sources for subsequent investigations.

For the retained sources, we compute the model-predicted NUV fluxes and compare them with the observed values (see Figure 1). We define the NUV flux ratio as $R_{\text{NUV}} = F_{\text{NUV,obs}}/F_{\text{NUV,mod}}$. 300 sources with $R_{\text{NUV}} \leq 1.2$ are considered to show no significant NUV excess and are directly retained. We note that some sources have $R_{\text{NUV}} < 1$, which is not physically expected and likely reflects measurement uncertainties or limitations of the model; no additional filtering is applied to these objects. For 550 sources with moderate excess, $1.2 < R_{\text{NUV}} \leq 3$, we perform further analysis to test whether the observed NUV emission can be explained by a non-degenerate companion or not.

To test this hypothesis, we model the companion in the moderate-excess systems as a main-sequence star. Stellar parameters for the companion are inferred from `Isochrones`⁵ (T. D. Morton 2015), adopting the same $[\text{Fe}/\text{H}]$ as the RGB in each system. The predicted parameters are used to generate synthetic spectra, which are then reddened using the SED-derived extinction and scaled by the distance to predict the observed fluxes and compute the corresponding NUV fluxes. We then compare the total model-predicted NUV fluxes of the RGB and the companion with the observed values (see Figure 2). We find a strong positive correlation between the predicted-to-observed NUV flux ratio and the previously provided companion mass, as expected if the companion were a normal luminous star. For a substantial fraction of sources, the total model flux exceeds the observed NUV flux by more than an order. Such large discrepancies are difficult to reconcile with measurement uncertainties or model limitations, indicating that a non-degenerate luminous companion is unlikely. We therefore interpret 479 systems with $F_{\text{NUV,tot,mod}}/F_{\text{NUV,obs}} \geq 10$ as more consistent with hosting dark companions and retain them as candidate BH/NS binaries. After applying both the SED quality selection and the UV consistency tests, we are left with 779 sources in the final sample.

4. GALACTIC KINEMATIC DIAGNOSTICS

We characterize the kinematic properties of 1,133 sources, whose optical-to-infrared SEDs can be well fitted by single-star model, by deriving their V_{pec} and maximum vertical heights above/below the Galactic plane ($|Z|_{\text{max}}$) in the

³ <https://svo2.cab.inta-csic.es/theory/fps/>

⁴ <https://github.com/mfouesneau/pystellib>

⁵ <https://isochrones.readthedocs.io/en/latest/index.html>

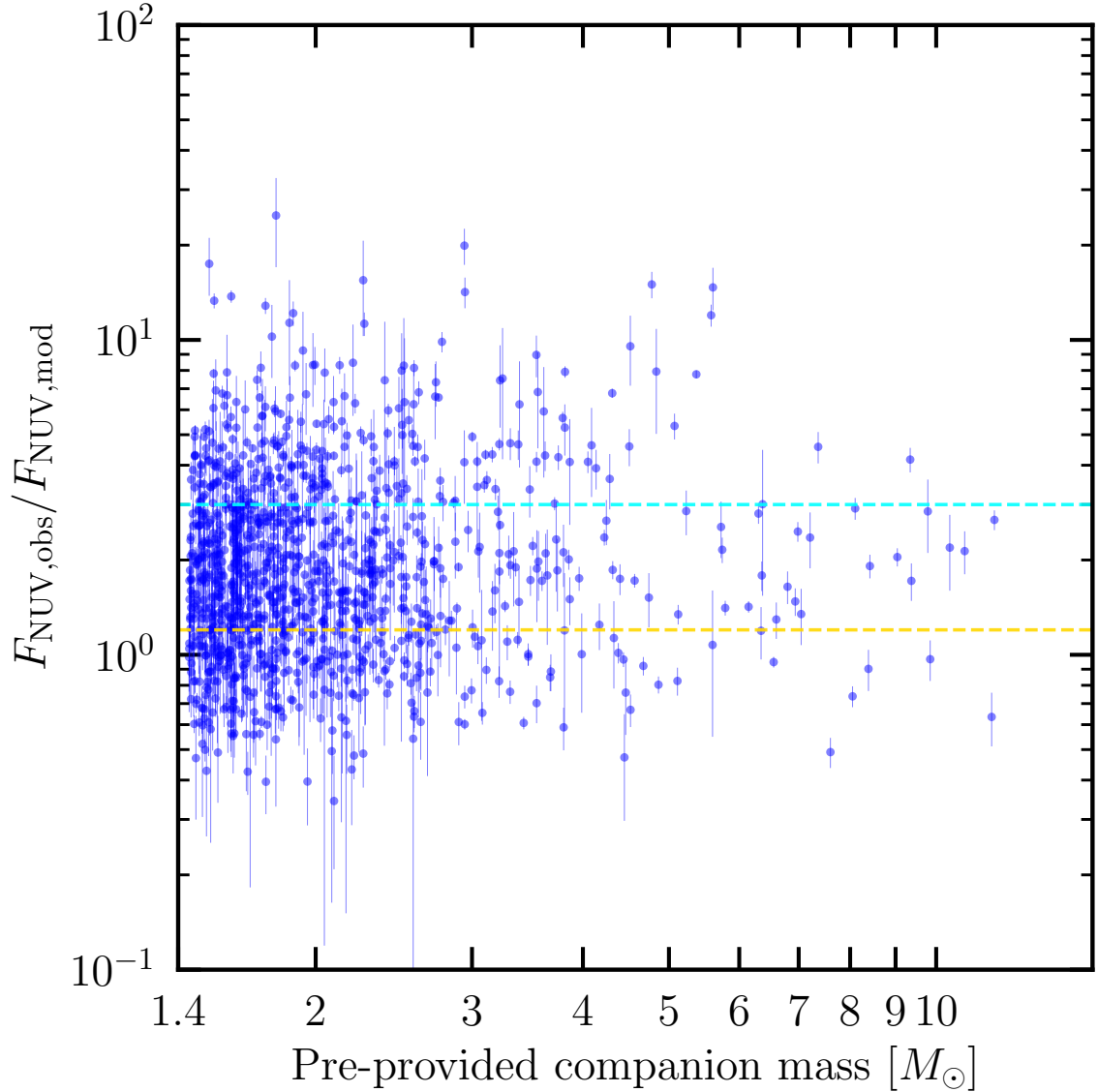


Figure 1. The ratio of observed NUV flux to model-predicted NUV flux as a function of the previously provided companion mass. The horizontal orange dashed line marks $F_{\text{NUV,obs}}/F_{\text{NUV,mod}} = 1.2$, below which sources are considered to show no significant NUV excess and are directly retained. Sources with moderate excess, $1.2 < F_{\text{NUV,obs}}/F_{\text{NUV,mod}} \leq 3$, indicated by the area between the cyan dashed line and orange dashed line, are subjected to further analysis allowing for a luminous stellar companion.

Galactic potential. We evaluate the V_{pec} at the Galactic-plane crossing phase ($Z = 0$). This choice provides a uniform kinematic reference across the sample, where the local circular velocity is well defined in the adopted Galactic potential model, and simultaneously reduces sensitivity to orbital-phase-dependent exchange between kinetic and gravitational potential energies. Systemic velocities needed for V_{pec} calculation are taken from `radial_velocity` published by *Gaia* DR3, which are derived from multi-epoch RV observations and provided as a robust average value for each source. Therefore, the use of *Gaia* DR3 `radial_velocity` as systemic velocities is reasonable. We integrate the orbits backward for 1 Gyr in the Galactic potential under the Milky Way potential model `McMillan17` (P. J. McMillan 2017), the most used Milky Way potential model, implemented by python package `galpy` (J. Bovy 2015), to determine the Galactic plane crossing phase and $|Z|_{\text{max}}$. Then we calculate the 3D velocities in Galactocentric Cartesian frame (V_x , V_y , and V_z) at the Galactic plane crossing phase. In the calculation process, we place the Sun at $(X, Z) = (-8.178, 0.025)$ kpc (J. Bland-Hawthorn & O. Gerhard 2016; GRAVITY Collaboration et al. 2019). At such place, the circular

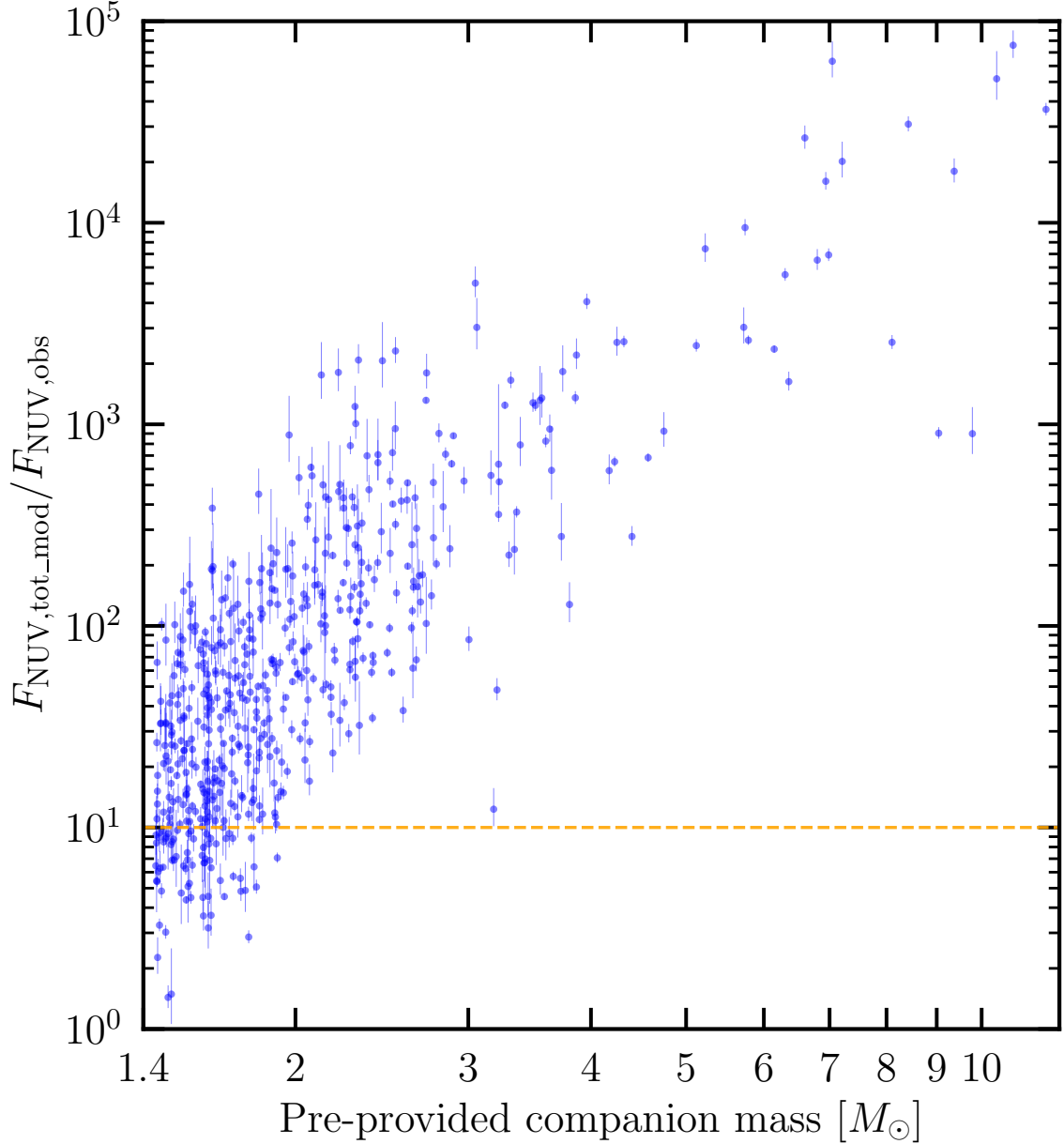


Figure 2. The ratio of total model-predicted NUV flux to observed NUV flux as a function of the previously provided companion mass. The horizontal orange dashed line marks $F_{\text{NUV,tot_mod}}/F_{\text{NUV,obs}} = 10$, above which the predicted flux from a non-degenerate luminous companion severely exceeds the observed value, making such companions unlikely.

velocity is set to be 233.2 km s^{-1} according to McMillan17. V_{pec} of the Sun relative to the Local Standard of Rest is set to be $(U_{\odot}, V_{\odot}, W_{\odot}) = (7.01, 10.13, 4.95) \text{ km s}^{-1}$ (Y. Huang et al. 2015). We convert V_x , V_y , and V_z into 3D Galactic space velocity (U, V, W) by the following matrix transformation:

$$\begin{bmatrix} -\cos \alpha & -\sin \alpha & 0 \\ -\sin \alpha & \cos \alpha & 0 \\ 0 & 0 & 1 \end{bmatrix} \begin{bmatrix} V_x \\ V_y \\ V_z \end{bmatrix} = \begin{bmatrix} U \\ V \\ W \end{bmatrix},$$

where α is the angle between the Galactic Center-to-source vector and the positive X-axis in Galactocentric Cartesian frame. From the resulting Galactic velocity components, we define the V_{pec} as $V_{\text{pec}} = \sqrt{U^2 + (V - V_c)^2 + W^2}$, where V_c is the local circular velocity at the disk-crossing radius.

Y. Zhao et al. (2026) investigated V_{pec} of compact-object binaries and major contaminating populations. By comparing their empirical cumulative distributions, they showed that the V_{pec} of more than 90% of contaminating sources lie below 100 km s^{-1} (see their Figure 3). We therefore adopt $V_{\text{pec}} \geq 100 \text{ km s}^{-1}$ to isolate systems probably accelerated by supernova natal kicks, yielding 216 sources. Among them, 176 sources also satisfy the SED-based selection criteria and 19 are BH candidates with previously provided masses $\geq 3 M_{\odot}$. On the other hand, theoretical studies suggest that BHs may experience substantially reduced natal kicks due to strong fallback (e.g. A. Tiwari et al. 2024) or even form via direct collapse with negligible mass ejection (e.g. C. L. Fryer 1999), naturally leading to lower V_{pec} . Therefore, 73 sources that satisfy the SED criterion alone and have previously provided companion masses $\geq 3 M_{\odot}$ remain plausible BH binary candidates.

In Figure 3, we respectively compare V_{pec} with previously provided companion mass, R_{NUV} , and $|Z|_{\text{max}}$, for sources with a goodness-of-fit probability $p > 0.05$. According to the previously provided companion masses, we divide the systems into NS-like zone, transition zone, and BH-like zone, respectively corresponding to previously provided companion mass of $\leq 2 M_{\odot}$, $< 2 M_{\odot}$ and $< 3 M_{\odot}$, and $\geq 3 M_{\odot}$. These three zones contain 677, 322, and 134 sources, respectively. The NS-like zone extends to higher V_{pec} tails than the BH-like zone; however, given the much larger sample size in the low-mass bin and possible selection effects, our data do not permit a quantitative comparison of natal kick distributions between the two populations. We further note a mild tendency for systems with higher V_{pec} to exhibit lower NUV flux ratios, with the median R_{NUV} shifting from ~ 2 at $V_{\text{pec}} < 100 \text{ km s}^{-1}$ to ~ 1.25 at higher V_{pec} . This behavior is consistent with kinematically heated systems preferentially hosting compact companions, while more significant NUV excess is more common among kinematically cold populations. Interestingly, the median R_{NUV} shifting in the subsample with $V_{\text{pec}} \geq 100 \text{ km s}^{-1}$, ~ 1.25 , matches the threshold adopted in Section 3 for identifying sources showing no significant NUV excess, providing an independent consistency check between the UV and kinematic diagnostics. Furthermore, a clear positive correlation is observed between V_{pec} and $|Z|_{\text{max}}$, indicating progressively heated orbits from disk-like to halo-like kinematics.

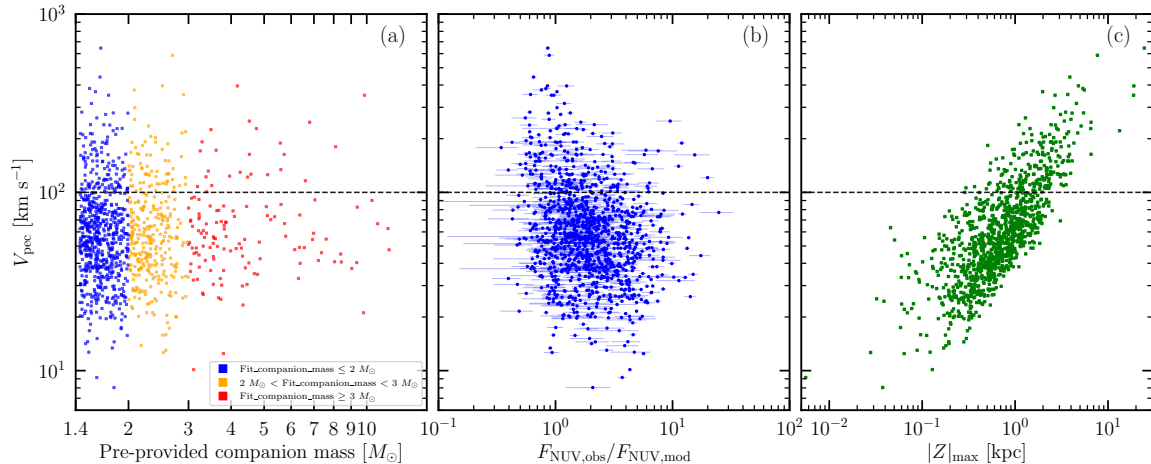


Figure 3. (a), V_{pec} as a function of the previously provided companion mass. NS-like zone, transition zone, and BH-like zone are respectively indicated by blue squares, orange squares and red squares. (b), V_{pec} as a function of R_{NUV} . (c), V_{pec} as a function of $|Z|_{\text{max}}$. In all panels, the horizontal black dashed line marks $V_{\text{pec}} = 100 \text{ km s}^{-1}$, above which sources are considered to be probably accelerated by supernova natal kicks. For NS-like zone, transition zone, and BH-like zone, there are 123, 68, and 25 systems that satisfy this criterion, respectively.

5. SUMMARY AND DISCUSSION

J. Müller-Horn et al. (2025) employed a forward-modeling framework, simulating *Gaia* observables for 21,028 RGB stars to target compact object candidates. According to their results, we perform SED and Galactic kinematic diagnostics for 1,328 dormant BH/NS binary candidates to assess their reliability and to prioritize targets for follow-up observations. A total of 779 sources satisfy the SED-based selection criteria. Their optical and infrared photometry can be well fitted by a single-star model and exhibit no UV excess or moderate UV excess that is completely insufficient to accommodate the existence of non-degenerate companions. Independent of the SED-based diagnostics, 216 sources

Table 1. Priority and secondary-priority candidates

<i>Gaia</i> DR3	Degrees of freedom	Reduced χ^2	R_{NUV}	$F_{\text{NUV,tot_mod}}/F_{\text{NUV,obs}}$	V_{pec}	$ Z _{\text{max}}$	Fit_comp_mass
ID					(km s $^{-1}$)	(kpc)	(M_{\odot})
413801205418517760	9	1.09	0.97 ± 0.14	$981.65^{+169.98}_{-126.26}$	350.83	18.83	$9.85^{+6.60}_{-3.95}$
4569884068106889088	9	0.88	2.92 ± 0.23	$2552.29^{+221.12}_{-188.47}$	180.23	3.13	$8.10^{+5.90}_{-3.41}$
2799283010053799936	9	1.27	1.64 ± 0.20	$6526.79^{+876.24}_{-690.77}$	247.51	6.56	$6.80^{+6.58}_{-3.34}$
4348345531815266688	9	1.41	1.29 ± 0.17	$26362.17^{+4014.72}_{-3077.40}$	116.10	1.12	$6.61^{+5.15}_{-2.89}$
6215201892206723712	9	1.12	2.55 ± 0.52	$3029.39^{+773.56}_{-512.05}$	163.16	1.97	$5.72^{+5.12}_{-2.70}$
4370292986492417280	9	1.16	1.07 ± 0.53	$5261.88^{+5052.29}_{-1730.04}$	134.10	0.76	$5.60^{+5.14}_{-2.68}$
5189794217106440192	7	1.75	1.34 ± 0.10	$2458.69^{+188.68}_{-163.58}$	125.51	1.40	$5.12^{+5.67}_{-2.69}$
4696396379961787520	9	1.22	1.52 ± 0.30	$924.86^{+224.55}_{-151.15}$	227.87	6.52	$4.75^{+7.00}_{-2.83}$
2431937996280114304	9	0.48	1.72 ± 0.09	$683.50^{+35.97}_{-32.55}$	126.54	2.93	$4.57^{+4.72}_{-2.32}$
4775580703429027328	9	0.45	0.67 ± 0.08	$3809.53^{+513.92}_{-404.72}$	163.42	3.86	$4.53^{+3.72}_{-2.04}$
6082713592919774336	9	0.67	0.76 ± 0.20	$7877.45^{+2852.63}_{-1654.42}$	121.86	1.16	$4.47^{+4.48}_{-2.24}$
6857124646247102720	9	1.69	2.67 ± 0.44	$2549.82^{+499.82}_{-359.06}$	129.80	2.60	$4.25^{+3.08}_{-1.79}$
6903875257889043200	9	0.67	1.25 ± 0.21	$589.25^{+119.59}_{-85.06}$	395.22	18.97	$4.17^{+4.99}_{-2.27}$
6461298879698884736	9	0.67	1.75 ± 0.15	$4061.55^{+390.61}_{-327.60}$	123.32	1.33	$3.96^{+5.46}_{-2.29}$
5690035586423107072	9	1.37	2.22 ± 0.15	$1241.30^{+89.20}_{-77.99}$	109.12	0.90	$3.51^{+3.60}_{-1.78}$
984731689102817408	9	0.84	1.73 ± 0.19	$1279.71^{+157.51}_{-126.40}$	224.82	2.90	$3.49^{+5.17}_{-2.08}$
830954817485226240	9	0.49	0.61 ± 0.03	$938.59^{+45.03}_{-41.09}$	131.67	2.18	$3.43^{+2.66}_{-1.50}$
2689755154957920896	8	1.13	1.12 ± 0.07	$153.41^{+9.55}_{-8.49}$	122.22	3.07	$3.38^{+2.77}_{-1.52}$
4624140465810214784	9	0.64	1.10 ± 0.14	$355.87^{+52.07}_{-40.28}$	191.81	3.06	$3.29^{+4.63}_{-1.92}$
...

Notes: column(1): *Gaia* DR3 solution ID; column(2): Degrees of freedom in SED fitting; column(3): Reduced χ^2 of the SED fitting; column(4): the ratio of observed NUV flux to model-predicted NUV flux (the Y-axis in Figure 1); column(5): the ratio of total model-predicted NUV flux to observed NUV flux (the Y-axis in Figure 2); column(6): Peculiar velocity calculated in Section 4; column(7): The maximum vertical height above/below the Galactic plane calculated in Section 4; column(8): The fitted companion mass provided by [J. Müller-Horn et al. \(2025\)](#). Only 19 highest-priority BH candidates are listed here and the complete table is available in the online journal and at CDS.

meet the kinematic criterion with $V_{\text{pec}} \geq 100$ km s $^{-1}$. We identify the intersection of these two samples as the highest-priority candidates for follow-up observations. The highest-priority candidates contain 176 sources, of which 19 are BH candidates with previously provided masses $\geq 3 M_{\odot}$. Besides, we designate 73 sources that satisfy the SED criterion alone and have previously provided companion masses $\geq 3 M_{\odot}$ as a secondary-priority sample which only contains BH candidates. Both the highest-priority and secondary-priority candidates are listed in Table 1.

Hierarchical systems may contaminate both the highest-priority and secondary-priority samples since they are (ultra-)wide systems that are enough to accommodate inner binaries. The high V_{pec} of the highest-priority candidates indicates a comparatively higher likelihood of having experienced supernova explosions. Consequently, even if such systems host inner binaries, they are expected to contain at least one compact object (BH or NS) rather than being composed purely of non-degenerate stars. In contrast, the secondary-priority sample, with lower V_{pec} , is more likely to be contaminated by hierarchical systems consisting of pure non-degenerate binaries that have not undergone supernova events. This distinction reflects a fundamental physical difference between the two samples. Within the secondary-priority candidates, systems with higher previously provided companion masses or comparatively higher V_{pec} are therefore comparatively more promising sources for follow-up observations.

ACKNOWLEDGMENTS

We thank Jifeng Liu, Yang Huang, and Zhi-Xiang Zhang for helpful discussion. This work was supported by the National Key R&D Program of China under grants 2023YFA1607901 and 2021YFA1600401, the National Natural Science Foundation of China under grants 12433007 and 12221003. We acknowledge the science research grants from the China Manned Space Project with No. CMS-CSST-2025-A13. This work has made use of data from the European Space Agency (ESA) mission Gaia (<https://www.cosmos.esa.int/gaia>), processed by the Gaia Data Processing and Analysis Consortium (DPAC, <https://www.cosmos.esa.int/web/gaia/dpac/consortium>). Funding for the DPAC has been provided by national institutions, in particular the institutions participating in the Gaia Multilateral Agreement. This paper includes data collected by the TESS mission. Funding for the TESS mission is provided by the NASA's Science Mission Directorate. This publication makes use of data products from the Two Micron All Sky Survey, which is a joint project of the University of Massachusetts and the Infrared Processing and Analysis Center/California Institute of Technology, funded by the National Aeronautics and Space Administration and the National Science Foundation. Database access and other data services are provided by the Associação Laboratório Interinstitucional de e-Astronomia (LIneA) with the financial support from INCT do e-Universo (Processo No. 465376/2014-2). This work makes use of GALEX and 2MASS. This publication makes use of VOSA, developed under the Spanish Virtual Observatory (<https://svo.cab.inta-csic.es>) project funded by MCIN/AEI/10.13039/501100011033/ through grant PID2020-112949GB-I00. VOSA has been partially updated by using funding from the European Union's Horizon 2020 Research and Innovation Programme, under Grant Agreement No. 776403 (EXOPLANETS-A). This research has made use of the VizieR catalogue access tool, CDS, Strasbourg, France (DOI : 10.26093/cds/vizier). The original description of the VizieR service was published in 2000, A&AS 143, 23.

Software: Astropy ([Astropy Collaboration et al. 2013, 2018, 2022](#)), astroquery ([A. Ginsburg et al. 2019](#)), Numpy ([C. R. Harris et al. 2020](#)), Pandas ([T. pandas development team 2020](#)), matplotlib ([J. D. Hunter 2007](#)), emcee ([D. Foreman-Mackey et al. 2013](#)), Vizier ([F. Ochsenbein et al. 2000](#)), galpy ([J. Bovy 2015](#)), VOSA ([A. Bayo et al. 2008](#)), extinction ([K. Barbary 2016](#)), Isochrones ([T. D. Morton 2015](#)), pystellib (<https://github.com/mfouesneau/pystellib>), spectool ([zhang-zhixiang 2025](#))

REFERENCES

Abbott, B. P., Abbott, R., Abbott, T. D., et al. 2016, PhRvL, 116, 061102, doi: [10.1103/PhysRevLett.116.061102](https://doi.org/10.1103/PhysRevLett.116.061102)

Allard, F. 2016, in SF2A-2016: Proceedings of the Annual meeting of the French Society of Astronomy and Astrophysics, ed. C. Reylé, J. Richard, L. Cambrésy, M. Deleuil, E. Pécontal, L. Tresse, & I. Vauglin, 223–227

Allard, F., Hauschildt, P. H., Alexander, D. R., Tamanai, A., & Schweitzer, A. 2001, ApJ, 556, 357, doi: [10.1086/321547](https://doi.org/10.1086/321547)

Allard, F., Homeier, D., & Freytag, B. 2012, Philosophical Transactions of the Royal Society of London Series A, 370, 2765, doi: [10.1098/rsta.2011.0269](https://doi.org/10.1098/rsta.2011.0269)

Astropy Collaboration, Robitaille, T. P., Tollerud, E. J., et al. 2013, A&A, 558, A33, doi: [10.1051/0004-6361/201322068](https://doi.org/10.1051/0004-6361/201322068)

Astropy Collaboration, Price-Whelan, A. M., Sipőcz, B. M., et al. 2018, AJ, 156, 123, doi: [10.3847/1538-3881/aabc4f](https://doi.org/10.3847/1538-3881/aabc4f)

Astropy Collaboration, Price-Whelan, A. M., Lim, P. L., et al. 2022, ApJ, 935, 167, doi: [10.3847/1538-4357/ac7c74](https://doi.org/10.3847/1538-4357/ac7c74)

Barbary, K. 2016, extinction v0.3.0, Zenodo, doi: [10.5281/zenodo.804967](https://doi.org/10.5281/zenodo.804967)

Bayo, A., Rodrigo, C., Barrado Y Navascués, D., et al. 2008, A&A, 492, 277, doi: [10.1051/0004-6361:200810395](https://doi.org/10.1051/0004-6361:200810395)

Bianchi, L., Hutchings, J., Bohlin, R., Thilker, D., & Berti, E. 2024, ApJ, 976, 131, doi: [10.3847/1538-4357/ad712f](https://doi.org/10.3847/1538-4357/ad712f)

Blaauw, A. 1961, BAN, 15, 265

Bland-Hawthorn, J., & Gerhard, O. 2016, ARA&A, 54, 529, doi: [10.1146/annurev-astro-081915-023441](https://doi.org/10.1146/annurev-astro-081915-023441)

Bovy, J. 2015, ApJS, 216, 29, doi: [10.1088/0067-0049/216/2/29](https://doi.org/10.1088/0067-0049/216/2/29)

Cardelli, J. A., Clayton, G. C., & Mathis, J. S. 1989, ApJ, 345, 245, doi: [10.1086/167900](https://doi.org/10.1086/167900)

Corral-Santana, J. M., Casares, J., Muñoz-Darias, T., et al. 2016, A&A, 587, A61, doi: [10.1051/0004-6361/201527130](https://doi.org/10.1051/0004-6361/201527130)

El-Badry, K., Rix, H.-W., Quataert, E., et al. 2023a, MNRAS, 518, 1057, doi: [10.1093/mnras/stac3140](https://doi.org/10.1093/mnras/stac3140)

El-Badry, K., Rix, H.-W., Cendes, Y., et al. 2023b, MNRAS, 521, 4323, doi: [10.1093/mnras/stad799](https://doi.org/10.1093/mnras/stad799)

Fitzpatrick, E. L. 1999, PASP, 111, 63, doi: [10.1086/316293](https://doi.org/10.1086/316293)

Foreman-Mackey, D., Hogg, D. W., Lang, D., & Goodman, J. 2013, PASP, 125, 306, doi: [10.1086/670067](https://doi.org/10.1086/670067)

Fortin, F., Kalsi, A., García, F., Simaz-Bunzel, A., & Chaty, S. 2024, A&A, 684, A124, doi: [10.1051/0004-6361/202347908](https://doi.org/10.1051/0004-6361/202347908)

Fryer, C. L. 1999, ApJ, 522, 413, doi: [10.1086/307647](https://doi.org/10.1086/307647)

Gaia Collaboration, Vallenari, A., Brown, A. G. A., et al. 2023, A&A, 674, A1, doi: [10.1051/0004-6361/202243940](https://doi.org/10.1051/0004-6361/202243940)

Ginsburg, A., Sipőcz, B. M., Brasseur, C. E., et al. 2019, AJ, 157, 98, doi: [10.3847/1538-3881/aafc33](https://doi.org/10.3847/1538-3881/aafc33)

GRAVITY Collaboration, Abuter, R., Amorim, A., et al. 2019, A&A, 625, L10, doi: [10.1051/0004-6361/201935656](https://doi.org/10.1051/0004-6361/201935656)

Harris, C. R., Millman, K. J., van der Walt, S. J., et al. 2020, Nature, 585, 357, doi: [10.1038/s41586-020-2649-2](https://doi.org/10.1038/s41586-020-2649-2)

Henden, A. A., Levine, S., Terrell, D., & Welch, D. L. 2015, in American Astronomical Society Meeting Abstracts, Vol. 225, American Astronomical Society Meeting Abstracts #225, 336.16

Hobbs, G., Lorimer, D. R., Lyne, A. G., & Kramer, M. 2005, MNRAS, 360, 974, doi: [10.1111/j.1365-2966.2005.09087.x](https://doi.org/10.1111/j.1365-2966.2005.09087.x)

Huang, Y., Liu, X. W., Yuan, H. B., et al. 2015, MNRAS, 449, 162, doi: [10.1093/mnras/stv204](https://doi.org/10.1093/mnras/stv204)

Hunter, J. D. 2007, Computing in Science & Engineering, 9, 90, doi: [10.1109/MCSE.2007.55](https://doi.org/10.1109/MCSE.2007.55)

Huson, D., Cowan, I., Sizemore, L., Kounkel, M., & Hutchinson, B. 2025a, ApJ, 984, 58, doi: [10.3847/1538-4357/adc2fa](https://doi.org/10.3847/1538-4357/adc2fa)

Huson, D., Cowan, I., Sizemore, L., Kounkel, M., & Hutchinson, B. 2025b, VizieR Online Data Catalog: Stellar parameters from XP and RVS spectra (Huson+ 2025), VizieR On-line Data Catalog: J/ApJ/984/58. Originally published in: 2025ApJ...984...58H

Janka, H.-T. 2013, MNRAS, 434, 1355, doi: [10.1093/mnras/stt1106](https://doi.org/10.1093/mnras/stt1106)

Jayasinghe, T., Stanek, K. Z., Thompson, T. A., et al. 2021, MNRAS, 504, 2577, doi: [10.1093/mnras/stab907](https://doi.org/10.1093/mnras/stab907)

Kochanek, C. S., Stanek, K. Z., Thompson, T. A., & Jayasinghe, T. 2025, arXiv e-prints, arXiv:2509.10608, doi: [10.48550/arXiv.2509.10608](https://doi.org/10.48550/arXiv.2509.10608)

Lyne, A. G., & Lorimer, D. R. 1994, Nature, 369, 127, doi: [10.1038/369127a0](https://doi.org/10.1038/369127a0)

Mahy, L., Sana, H., Shenar, T., et al. 2022, A&A, 664, A159, doi: [10.1051/0004-6361/202243147](https://doi.org/10.1051/0004-6361/202243147)

Manchester, R. N., Hobbs, G. B., Teoh, A., & Hobbs, M. 2005, AJ, 129, 1993, doi: [10.1086/428488](https://doi.org/10.1086/428488)

Martin, D. C., Fanson, J., Schiminovich, D., et al. 2005, ApJL, 619, L1, doi: [10.1086/426387](https://doi.org/10.1086/426387)

McMillan, P. J. 2017, MNRAS, 465, 76, doi: [10.1093/mnras/stw2759](https://doi.org/10.1093/mnras/stw2759)

Morrissey, P., Schiminovich, D., Barlow, T. A., et al. 2005, ApJL, 619, L7, doi: [10.1086/424734](https://doi.org/10.1086/424734)

Morton, T. D. 2015, isochrones: Stellar model grid package,, Astrophysics Source Code Library, record ascl:1503.010 <http://ascl.net/1503.010>

Müller-Horn, J., Rix, H.-W., El-Badry, K., et al. 2025, arXiv e-prints, arXiv:2510.05982, doi: [10.48550/arXiv.2510.05982](https://doi.org/10.48550/arXiv.2510.05982)

Ochsenbein, F., Bauer, P., & Marcout, J. 2000, A&AS, 143, 23, doi: [10.1051/aas:2000169](https://doi.org/10.1051/aas:2000169)

pandas development team, T. 2020, pandas-dev/pandas: Pandas, latest Zenodo, doi: [10.5281/zenodo.3509134](https://doi.org/10.5281/zenodo.3509134)

Ricker, G. R., Winn, J. N., Vanderspek, R., et al. 2015, Journal of Astronomical Telescopes, Instruments, and Systems, 1, 014003, doi: [10.1117/1.JATIS.1.1.014003](https://doi.org/10.1117/1.JATIS.1.1.014003)

Sahu, K. C., Anderson, J., Casertano, S., et al. 2025, ApJ, 983, 104, doi: [10.3847/1538-4357/adbe6e](https://doi.org/10.3847/1538-4357/adbe6e)

Sartore, N., Ripamonti, E., Treves, A., & Turolla, R. 2010, A&A, 510, A23, doi: [10.1051/0004-6361/200912222](https://doi.org/10.1051/0004-6361/200912222)

Skrutskie, M. F., Cutri, R. M., Stiening, R., et al. 2006, AJ, 131, 1163, doi: [10.1086/498708](https://doi.org/10.1086/498708)

The LIGO Scientific Collaboration, the Virgo Collaboration, the KAGRA Collaboration, et al. 2025, arXiv e-prints, arXiv:2508.18079, doi: [10.48550/arXiv.2508.18079](https://doi.org/10.48550/arXiv.2508.18079)

Thompson, T. A., Kochanek, C. S., Stanek, K. Z., et al. 2019, Science, 366, 637, doi: [10.1126/science.aau4005](https://doi.org/10.1126/science.aau4005)

Timmes, F. X., Woosley, S. E., & Weaver, T. A. 1996, ApJ, 457, 834, doi: [10.1086/176778](https://doi.org/10.1086/176778)

Tiwari, A., Vijaykumar, A., Kapadia, S. J., Fragione, G., & Chatterjee, S. 2024, MNRAS, 527, 8586, doi: [10.1093/mnras/stad3749](https://doi.org/10.1093/mnras/stad3749)

Wang, S., Zhao, X., Feng, F., et al. 2024, Nature Astronomy, 8, 1583, doi: [10.1038/s41550-024-02359-9](https://doi.org/10.1038/s41550-024-02359-9)

Wright, E. L., Eisenhardt, P. R. M., Mainzer, A. K., et al. 2010, AJ, 140, 1868, doi: [10.1088/0004-6256/140/6/1868](https://doi.org/10.1088/0004-6256/140/6/1868)

Wyrzykowski, Ł., Kostrzewska-Rutkowska, Z., Skowron, J., et al. 2016, MNRAS, 458, 3012, doi: [10.1093/mnras/stw426](https://doi.org/10.1093/mnras/stw426)

Yi, T., Gu, W.-M., Zhang, Z.-X., et al. 2022, Nature Astronomy, 6, 1203, doi: [10.1038/s41550-022-01766-0](https://doi.org/10.1038/s41550-022-01766-0)

zhang-zhixiang. 2025, zhang-zhixiang/spectool: spectool version 1.0.1, v1.0.1 Zenodo, doi: [10.5281/zenodo.14947417](https://doi.org/10.5281/zenodo.14947417)

Zhao, Y., Gandhi, P., Knigge, C., et al. 2026, MNRAS, doi: [10.1093/mnras/stag058](https://doi.org/10.1093/mnras/stag058)